Pack aluminization of nickel anode for molten carbonate fuel cells

H.S. Chun[a,*], G.P. Park[a], J.H. Lim[a], K. Kim[d], J.K. Lee[b], K.H. Moon[c] and J.H. Youn[c]

[a]*Department of Chemical Engineering, Korea University, 1 Anam-dong, Sungbuk-ku, Seoul 136-701 (Korea)*

[b]*Department of Environmental Engineering, National Fisheries, University of Pusan, Daeyeon-dong, Nam-ku Pusan 608-737 (Korea)*

[c]*Energy R&D Team, Living Research Center, Samsung Electronics Co., Ltd., 416 Maetan dong, Paldal-Gu, Suwon 441-742 (Korea)*

[d]*Department of Chemistry, Korea University, 1 Anam-dong, Sungbuk-ku, Seoul 136-701 (Korea)*

Abstract

The aluminum pack cementation (pack aluminization) process on a porous nickel anode for molten carbonate fuel cells has been studied to improve anode creep resistance. The porous nickel substrates used in this study were fabricated by doctor blade equipment followed by sintering (850 °C). Packs surrounding the Ni anode were made by mixing Al_2O_3 powder, Al powder, and NaCl as activator. The pack aluminization was performed at 700 to 850 °C for 0.5–5.0 h. After pack aluminization, the principal Ni–Al intermetallic compounds detected were Ni_3Al at 700 °C, NiAl at 750 °C and Ni_3Al_2 at 800 °C. The aluminum content in the aluminized Ni anode was proportional to the square root of pack aluminizing time. With increasing the Al content in the anode, the creep of the anode decreased. It was nearly constant (2.0%) when the Al content was above 5.0%. Although the exchange current density (24 mA/cm^2) for the aluminized (2.5 wt.%) Ni anode was somewhat lower than that of the pure Ni anode (40 mA/cm^2), the performance of a single cell using an aluminized Ni anode was similar to that of the one with pure Ni anode.

Introduction

Molten carbonate fuel cells (MCFCs) have high efficiency which results from their low polarization, their high-grade waste heat, and their ability for internal reforming. The overall plant cost of the MCFC may be lower than that of the phosphoric acid full cell (PAFC) since fuel processing systems should be less complex, due to the absence of system required for removing CO, and of the requirement for noble metal catalysts. Porous MCFC nickel anodes are susceptible to creep at 650 °C, due to the weight of the stack itself and to the pressure required for improving the contact of each cell element. The electrode creep occurs namely by a combination of at least three different mechanisms: particle rearrangement, sintering, and dislocation movement. The creep resistance of the anode structure may be significantly improved by using additives such as Cr, Co, Al and Mg.

*Author to whom correspondence should be addressed.

SSDI 0378-7753(93)01815-Y

Standard anodes have usually been of Ni–Cr (10%) type. These show some creep (5–10%, in 100 h at 650 °C and under 100 psi load). Their pore-size distribution may also change during operation. This creep can result in a poor contact, high anode overvoltage and fuel gas leakage [1]. Cell performance may also be lowered due to the change of pore-size distribution [2]. Hence, adding Al to the Ni or Ni–Cr anode has been studied to make creep lower than 5.0% and to maintain constant pore-size distribution during operation [3–7].

A typical fabrication process for porous Ni–Al anodes involves slurry casting of a mixture of Ni–Al alloy particles, binder and solvent, which is followed by drying, burn-out and sintering. This method can use the same process as that for pure Ni anode fabrication. However, micro Ni–Al alloy particles are difficult to prepare. Hence, pack cementation was selected as a method which permits Al to deposit uniformly on a porous Ni anode. Pack cementation is a process in which a chemical vapour deposition (CVD) process takes place with substrates surrounded by a reactive pack. The pack consists of the Al to be deposited, Al_2O_3 as an inert filler to prevent sintering, and a halide (NH_4Cl, NH_4I, NaCl) as the active agent.

Many investigations on pack aluminization of nonporous Ni or Ni alloy substrates have been carried out [8–14], but the study of pack aluminization on porous Ni substrate has never been reported. In this paper, the effects of the variation of temperature and time on the pack aluminization of porous Ni anodes and the characteristics of pack-aluminized MCFC Ni anodes was studied.

Experimental

Porous nickel substrate fabrication

Green sheet was made by casting a slurry of Inco 255 Ni powder (average particle size: ~3 μm), polyvinyl butyral (PVB), a solvent (toluene/ethanol) and dibutyl phthalate (DBP) using a doctor blade unit. After drying at room temperature the sheet was burnt out at 400–500 °C for 2.0 h in air to remove the binder, which was followed by sintering at 850 °C for 15 min in 20% H_2/80% N_2. The sintered Ni anode had ~80% porosity and 0.9 mm thickness. After washing with ethanol and distilled water, the Ni substrate was dried and used for pack aluminization.

Pack aluminization procedure

The pack consisted of 25 wt.% Al powder (ALCOA, average particle size: 6–9 μm), 5% NaCl (SHINYO, 99.9% pure) and Al_2O_3 power (ALCOA, average particle size: 5 μm). Approximately 10 g of pack was placed in an alumina crucible. Nickel anode substrates were placed in the pack, and a slide-fitting cover was set on the crucible. The crucible was put in the furnace mouth whose temperature was always maintained below 300 °C, where no reaction could proceed. The crucible was moved to the center of the furnace, when the desired temperature (700–850 °C) was reached. This was maintained for 0.5–5.0 h. A gas flow of 20% H_2/80% Ar was maintained at 100 ml/min throughout the process. The aluminized anode was removed from the powder, rinsed in distilled water, dried and weighed to determine the deposited aluminum content.

Analysis of aluminized Ni anodes

Phase identification was verified by X-ray diffraction (Rigaku, 40 kV, 40 mA, Cu Kα). Observation was also carried out using a scanning electron microscope (Hitachi,

Ltd.) operating with an incident electron beam of 20 kV. The porosity and pore-size distribution of the anodes were measured by a Hg porosimeter (Micromeritics, model 9220).

Creep test

Creep tests were performed in the apparatus shown in Fig. 1. An anode gas mixture was maintained by flowing 60% H_2/40% CO_2 humidified at 60 °C. Cast sheets containing carbonate needed to fill, 25% of the electrode pore volume were placed between the anode samples. Tests were performed at 650 °C and 100 psi over 100 h.

Half-cell test

The working electrodes were pure Ni plates (99.995%, Material Research Co.) and aluminized Ni anode (Al 2.5 wt.%) selected from the aluminized specimens. The counter electrode was a gold sheet fitted as an inner liner to the alumina crucible to entirely surround the working electrode ensuring uniform current distribution [15]. A gold wire in equilibrium with a 33.3% O_2/66.7% CO_2 gas mixture inside an alumina tube served as reference electrode. Electrolyte in the reference electrode tube connected with the bulk through a small (0.4 mm diameter) hole at the bottom. The flow rate of the anode gas (40% H_2/40% CO_2/20% H_2O) was maintained at 100 ml/min. The working electrode potential was controlled by a potentiostat (EG&G, Princeton Applied Research, model 273). Steady-state currents were recorded on an x-y recorder (Yokogawa, model 3056). To eliminate errors caused by mass-transfer effects, transient potentiostatic techniques were used.

Single-cell test

To compare performance, the porous pure Ni anode and the aluminized porous Ni anode (Al 7.2 wt.%) were used in single cell tests. The cathode was a porous NiO plate and electrolyte was Li_2CO_3/K_2CO_3 (62/38 m/o) eutectic impregnated in a $LiAlO_2$ matrix. The effective electrode area was 1.2 cm^2, and the single cell was pressed at 30 psi to give a good contact. It was operated at a constant current density of 150 mA/cm^2, using a fuel gas (68% H_2/12% CO_2/20% H_2O) and a (60% CO_2/40% O_2) cathode gas for 100 h.

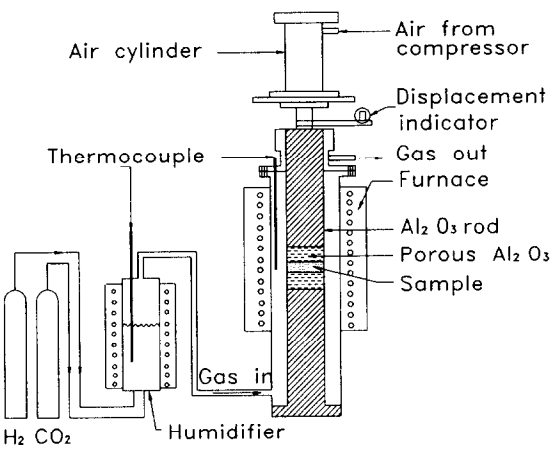

Fig. 1. Schematic diagram of the creep test apparatus.

Results and discussion

Since evaporative weight loss (Ni vapor pressure at 700 °C: 10^{-12} atm) was 1.3×10^{-5} g under the experimental conditions (H_2/N_2 gas mixture: 100 ml/min, flow for 10 h at 700 °C), any error due to evaporation of Ni was negligible [16].

Phase and structure of anode surface

Microstructures of anodes aluminized for 2.0 h in packs at 700 and 800 °C are shown in Fig. 2. Ni–Al intermetallic grains were attached to Ni particles as shown in this Figure [12]. The structures became more consolidated after pack cementation at 750 °C compared with 700 °C. Thus, the sintering of Ni particles and the diffusion rate of aluminum become much faster as temperature increases.

X-ray diffraction patterns of aluminized substrates at various temperatures are shown in Fig. 3. After pack aluminization, Ni_3Al, NiAl and Ni_2Al_3 phases appeared at 700, 750 and 800 °C, respectively. As the temperature of pack aluminization increased, an Ni–Al intermetallic compound with a higher aluminum content appeared.

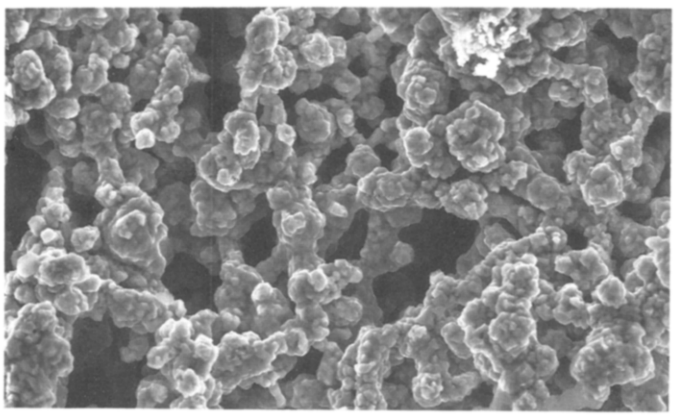

(a)

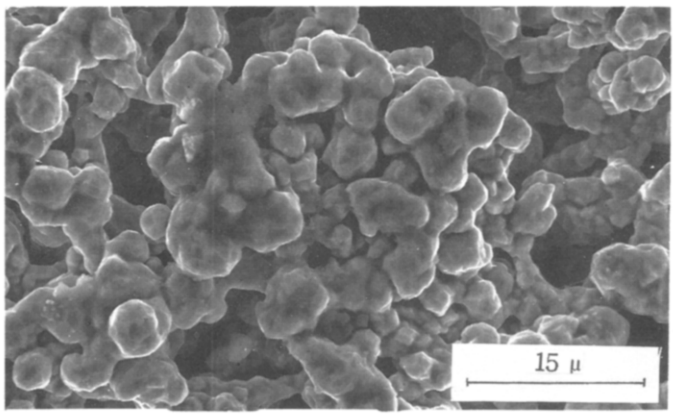

(b)

Fig. 2. Scanning electron micrographs of surfaces of the aluminized Ni anodes after pack cementation for 20 h: (a) 700 °C pack, and (b) 800 °C pack.

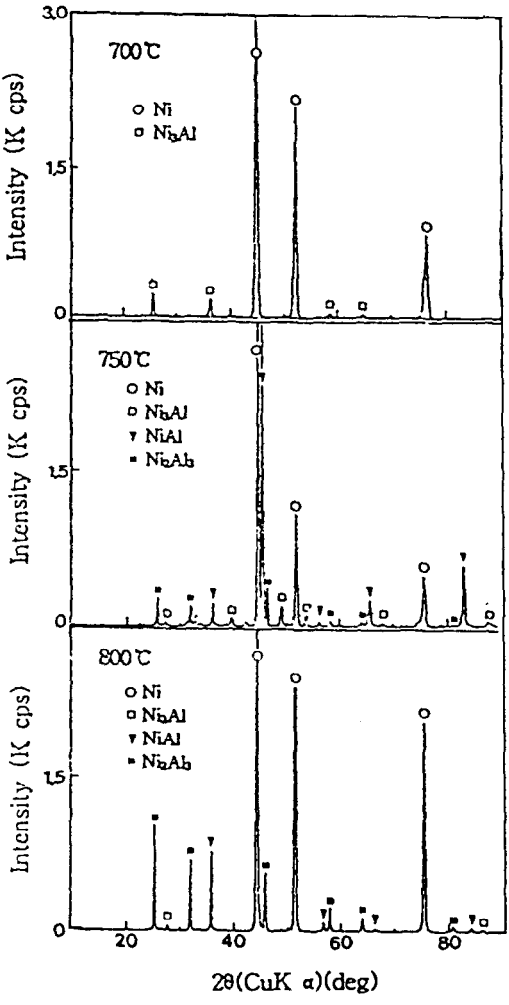

Fig. 3. X-ray diffractions of the aluminized Ni anode after pack aluminization at various temperatures.

Kinetics of pack aluminization

Aluminum weight gain data are plotted against aluminizing time in Fig. 4(a). Figure 4(b) is a plot of w^2 (weight gain) against aluminizing time assuming that parabolic kinetics ($w^2=kt$) apply. The plot suggests that parabolic kinetics applies to pack aluminization on both porous and nonporous substrates [10]. The parabolic rate constant at 750 °C was 2.08×10^{-3} mg^2 cm^{-4} s^{-1}. The experimental k was similar to the calculated value (1.60×10^{-3} mg^2 cm^{-4} s^{-1}) derived by Levine–Cave model for kinetics of aluminization on the nonporous nickel substrates [10]. The rate constant, k, according to the Levine–Caves model is given by the following equation:

$$k=\frac{2\rho\epsilon M}{lRT}\Sigma D_i(P_i-P_i') \tag{1}$$

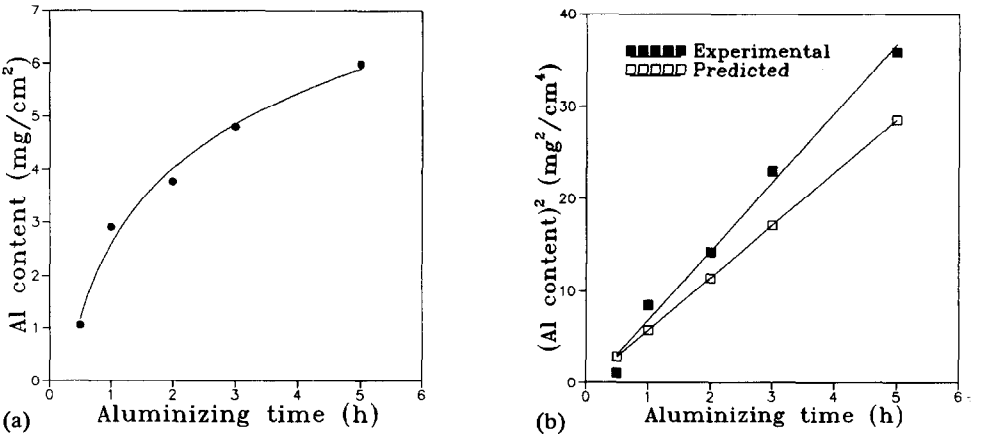

Fig. 4. Aluminum content in the aluminized Ni anodes as a function of pack aluminizing time at 750 °C: (a) Al weight gain data, and (b) weight gain data vs. time assuring that parabolic kinetics apply.

TABLE 1

Calculated partial pressures and diffusivities of reactive species at 750 °C

	AlCl	$AlCl_2$	$AlCl_3$
P (atm)	3.77×10^{-5}	8.72×10^{-7}	1.17×10^{-9}
P' (atm)	1.46×10^{-7}	1.32×10^{-9}	6.87×10^{-13}
D ($cm^2\ s^{-1}$)	0.8243	0.644	0.5439

[a]P = partial pressure at the bulk pack; P' = partial pressure at the aluminizing surface, and D = diffusivity at gas state.

where, ρ is the pack aluminum density in g cm^{-3}, ϵ and l are correction factors for pack porosity and pore length, D_i and P_i are the diffusivity and partial pressure of the ith aluminum bearing species, and M is atomic weight of aluminum. The partial pressures [17] and diffusivities used in this equation are given in Table 1.

The aluminum weight gain data are plotted against pack aluminizing temperature in Fig. 5. Since the kinetics of Al weight gain in a NaCl-activated pack fit a parabolic law, the activation energy of pack process can be obtained from the slope of ln w^2 versus $1/T$ plot at constant pack aluminizing time (here 2.0 h). The activation energy is 345 kJ mol^{-1} in the NaCl-activated pack at 700–850 °C. At 376.6 kJ mol^{-1} it is slightly lower for a nonporous substrate in a NaCl-activated pack at 982–1149 °C [10].

Porosity, pore-size distribution

Figure 6 shows the effect of Al contents on the porosity of pack aluminized anodes. This shows that aluminization on porous substrates lowers porosity.

The pore-size distributions as a function of the Al content in aluminized anodes are shown in Fig. 7, which indicates that the pore-size distribution is slightly changed with the Al content of the porous substrate. Figure 8 shows the pore-size distributions for an aluminized Ni anode (Al 5.9%) before and after a creep test, indicating that it has a good resistance to the change of pore-size distribution.

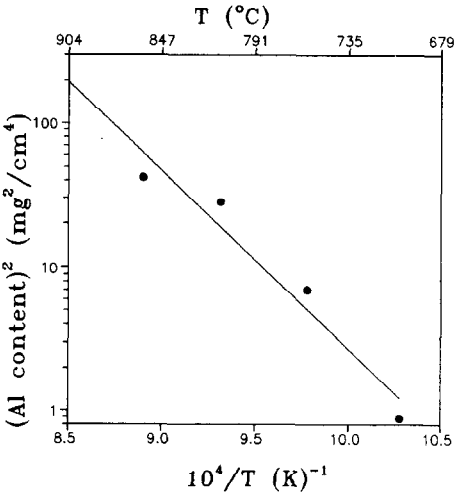

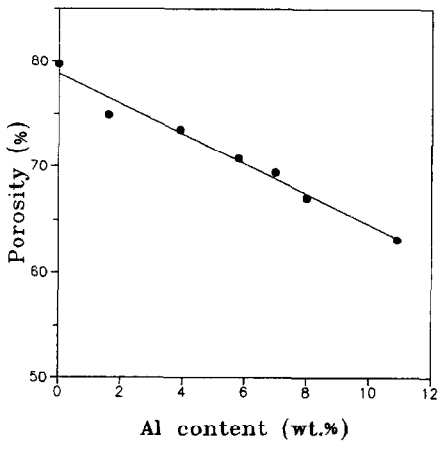

Fig. 5. Aluminum content in the aluminized Ni anodes as a function of aluminizing temperature (aluminizing time: 2.0 h).

Fig. 6. The variation of porosity with Al content in the aluminized Ni anodes.

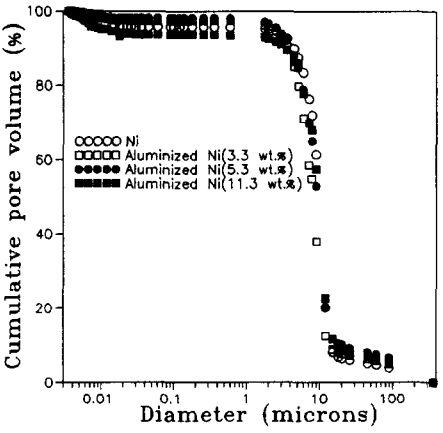

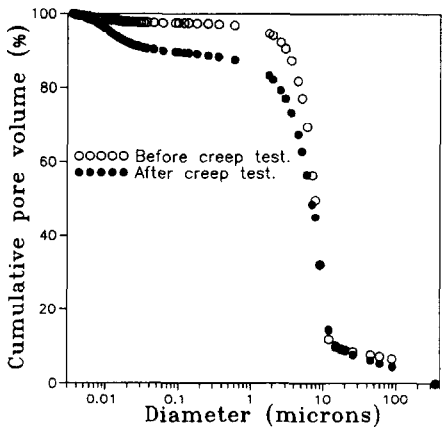

Fig. 7. Pore-size distributions of the aluminized Ni anodes as a function of Al content in the anodes.

Fig. 8. Comparison of pore-size distribution of the aluminized (5.9 wt.%) Ni anode before and after creep test. Creep test condition: in 53%H_2/27%CO_2/20%H_2O environment, 100 psi, and 100 h.

As location of gases–electrolyte interfaces in the electrodes and matrix are controlled by pore-size distribution in an operating fuel cell, substantial change in its parameters is undesirable.

Creep

Figure 9 shows the creep of aluminized Ni anodes as a function of Al content. Anode creep markedly decreased as the Al content increased to 5.0 wt.%, following

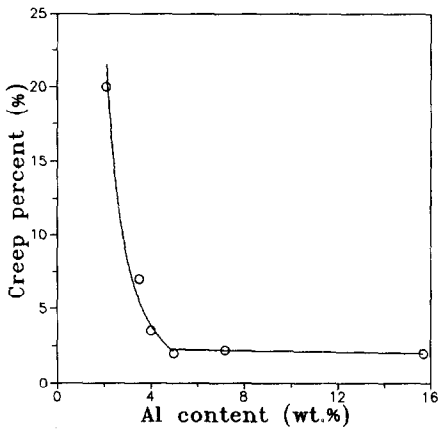

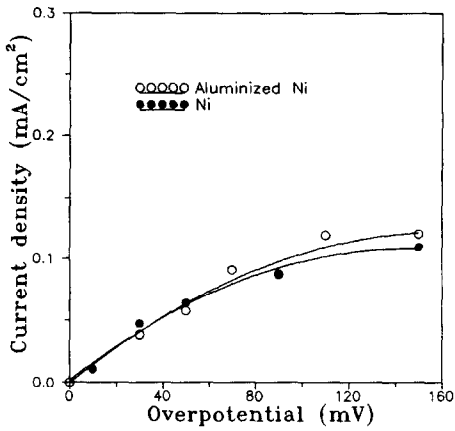

Fig. 9. The variation of creep with Al content in the aluminized Ni anodes. Creep test condition: in 53%H_2/27%CO_2/20%H_2O environment, 650 °C, 100 psi, and 100 h.

Fig. 10. Steady-state polarizations for the Ni anode and the aluminized (2.5 wt.%) Ni anode in Li_2CO_3/K_2CO_3 electrolyte; anode gas: 40%H_2/40%CO_2/20%H_2O, 650 °C.

which creep remained steady at about 2.0%. Aluminized Ni anodes showed low creep compared with that of Ni–Cr anodes (5–10%) reported in other studies [4].

Steady-state polarization and transient characteristics of the anode

Steady-state polarization curves for the pure Ni anode and of an aluminized Ni anode (Al 2.5%) in Li_2CO_3/K_2CO_3 eutectic at 650 °C are shown in Fig. 10. The current densities at the same overpotential are very similar in both cases. The anode-reaction rate on aluminized Ni was similar to that on pure Ni under mixed control (activation and mass-transfer) conditions [18]. To separate activation (kinetic) and mass-transfer polarization under mixed control conditions, a potential step was applied to the working electrode and the current was recorded as a function of time. The activation polarization may be obtained by extrapolation to time zero. For small times, Gerischer and Vielstich [19] showed that the current–time relationship for the reaction:

$$A = B + ze^- \tag{2}$$

is

$$i = i(0)(1 - 2k_f t^{1/2}/\pi^{1/2} D_A^{1/2}), \text{ for } k_f t^{1/2}/D_A^{1/2} \ll 1 \tag{3}$$

where $i(0)$ is the current density at time zero, k_f is the potential-dependent rate constant and D_A is the diffusivity of reactant. Thus, the current density is a linear function of $t^{1/2}$ for small time intervals. The current densities at time zero $i(0)$ were calculated by extrapolating currents between 0.3 and 0.5 ms to time zero as a function of $E^{1/2}$. The values obtained are presented in Fig. 11. The Butler–Volmer equation can be rewritten as:

$$\log \frac{i(0)}{\exp(\alpha_A + \alpha_C)\eta F/RT - 1} = \log i_0 - \frac{\alpha_C \eta F}{2.30\, RT} \tag{4}$$

to obtain an Allen–Hickling plot, where α_A and α_C are anodic- and cathodic-transfer coefficients (assuming $\alpha_A + \alpha_C = 2$), η is the overpotential and i_0 is the exchange-current

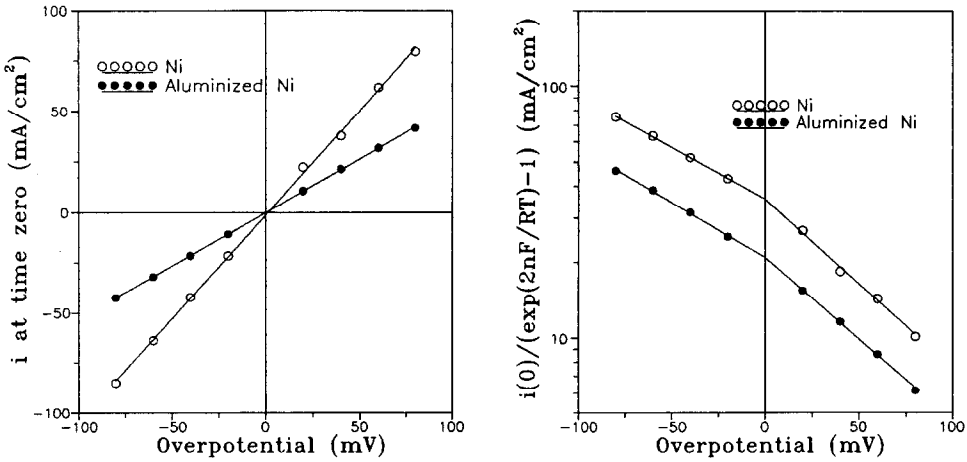

Fig. 11. Activation polarizations for the Ni anode and the aluminized (2.5 wt.%) Ni anode in the Li_2CO_3/K_2CO_3 electrolyte; anode gas: $40\%H_2/40\%CO_2/20\%H_2O$, 650 °C.

Fig. 12. Allen–Hickling plots for Ni anode and aluminized (2.5 wt.%) Ni anodes, anode gas: $40\%H_2/40\%CO_2/20\%H_2O$, 650 °C.

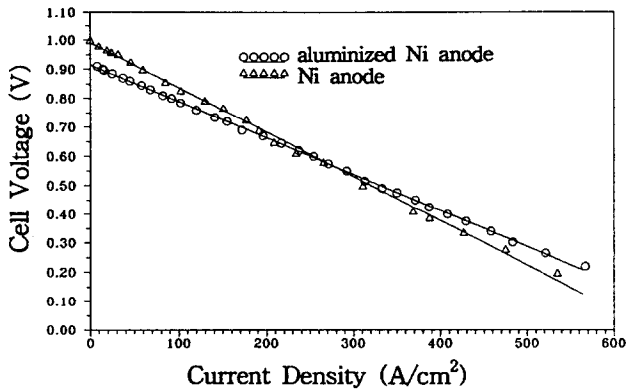

Fig. 13. Current–voltage curves for the sample cell with aluminized (7.2 wt.%) Ni anode after operation for 100 h; cathode: NiO; electrolyte: Li_2CO_3/K_2CO_3 (62/38 m/o); electrolyte matrix: $LiAlO_2$; temperature: 650 °C; anode gas: $68\%H_2/12\%CO_2/20\%H_2O$, and cathode gas: $60\%CO_2/40\%O_2$.

density. The Allen–Hickling plot derived according to eqn. (4) is shown in Fig. 12, and exchange-current densities of both anodes were obtained. The exchange-current density was found to be lower for aluminized Ni (24 mA cm^{-2}) than for pure Ni (40 mA cm^{-2}).

Single cell performance

After operation of 100 h the cell voltage remained at 0.9 V at 150 mA cm^{-2}. The relation between current density and cell voltage is shown in Fig. 13. There was no difference in the polarization behaviour of single cells using aluminized and standard

Ni anodes, based on measured *I–V* characteristics. It means that the anode reaction is diffusion controlled.

Conclusions

It was found that the rate of aluminization on a porous Ni substrate was governed by parabolic growth law ($w^2 = 3.12 \times 10^{14} \exp(-40460/T)t$). The Levine–Caves model accurately predicted the kinetics of aluminization on porous Ni substrates in NaCl activated pack.

Various Ni–Al intermetallic phases appeared at 700–850 °C in an NaCl-activated pack, improving the creep resistance of aluminized Ni-anodes. The aluminized anode maintained its pore-size distribution during creep test.

The exchange-current density at the aluminized Ni anode was somewhat lower than that of the Ni anode. However, steady-state polarization characteristics and single cell performance of the aluminized Ni anode was similar to that of the Ni anode, since the reaction was diffusion-controlled.

List of symbols

A	reactant
B	product
D_i	diffusivity of the ith species, cm^2 s^{-1}
D_A	diffusivity of reactant A, cm^2 s^{-1}
F	Faraday's constant, C mol^{-1}
i	current density, A cm^{-2}
$i(0)$	kinetic current density at time zero, A cm^{-2}
i_0	exchange current density, A cm^{-2}
k	rate constant, mg cm^{-4} s^{-1}
k_f	potential-dependent rate constant, cm s^{-1}
l	path length correction factor
M	atomic weight of aluminum, mg
P_i	partial pressure of the ith species in the bulk pack, atm
P_i'	partial pressure of the ith species at the aluminizing surface, atm
R	gas constant, J mol^{-1} K^{-1}
T	absolute temperature, K
t	time, s
w	aluminization weight, mg cm^{-2}
α_A	anodic-transfer coefficient
α_C	cathodic-transfer coefficient
ϵ	porosity
η	overpotential, V
ρ	pack aluminum concentration, mg cm^{-3}

References

1 K. Kinoshita, *ANL Rep. ANL-79-55,* Argonne National Laboratory, Argonne, IL, USA, 1979.
2 C.D. Iacovangelo, *J. Electrochem. Soc., 133* (1986) 2410–2416.
3 L. Plomp, J.B.J. Veldhuis, E.F. Sitters, F.P.F. van Berkel and S.B. van der Molden, *Proc. Int. Fuel Cell Conf., Makuhari, Japan, 1992,* pp. 157–160.

4 Y. Yamamasu, T. Kakihara, E. Kasai and T. Morita, *Proc. Int. Fuel Cell Conf., Makuhari, Japan, 1992,* pp. 161–164.
5 J. Tanaka, A. Saiai and S. Sakurada, *Proc. 3rd Int. Symp., Carbonate Fuel Cell Technology,* The Electrochemical Society, Pennington, NJ, USA, 1993, pp. 37–47.
6 Y. Miyake, K. Harima, T. Naakajima, Y. Aogagi, J. Tanaka and A. Saiai, *Proc. 3rd Int. Symp. Carbonate Fuel Cell Technology,* The Electrochemical Society, Pennington, NJ, USA, 1993, pp. 63–74.
7 T. Kahara, K. Ohtsuka, S. Takashima, M. Takeuchi, Y. Fukui and H. Fujimura, *Ext. Abstr., Fuel Cell Seminar, Tucsan, AZ, USA, 1992,* pp. 13–16.
8 H. Brill-Edwards and M. Epner, *Electrochem. Technol., 6* (1968) 299–307.
9 J.D. Gadd, J.F. Nejedlik and L.D. Graham, *Electrochem. Technol., 6* (1968) 307–315.
10 S.R. Levine and R.M. Caves, *J. Electrochem. Soc., 121* (1974) 1051–1064.
11 A.J. Hickl and R.W. Heckel, *Met. Trans., 6A* (1975) 431–440.
12 R. Sivakuma and L.L. Seigel, *Met. Trans., 7A* (1976) 1073–1079.
13 A. Thevand, S. Poize, J.P. Crousier and R. Streiff, *J. Mater. Sci., 16* (1981) 2467–2479.
14 B. Robert and A.R. Robert, *J. Electrochem. Soc., 140* (1993) 1181–1190.
15 S.H. Lu and J.R. Selman, *J. Electrochem. Soc., 131* (1984) 2827–2833.
16 D.R. Lide, *CRC Handbook of Chemistry and Physics,* CRC Press, Boston, 71st edn., 1990–1991, pp. 6–52.
17 D.R. Lide, Jr. (ed.), *JANAF Thermochemical Tables,* Vol. 14, Dow Chemical Co., Midland, MI, 3rd edn., 1985.
18 P.G.P. Ang and A.F. Sammells, *J. Electrochem. Soc., 127* (1980) 1287–1294.
19 H. Gerisher and W. Vielstich, *Z. Phys. Chem. N.F., 3* (1955) 16–33.